J. Phys. B: At. Mol. Opt. Phys. **31** (1998) 1553–1562. Printed in the UK PII: S0953-4075(98)87845-0

Single-electron loss and capture for 1.0–5.0 keV Ar^+ colliding with He

H Martínez

Instituto de Física, UNAM, Apdo Postal 48-3, 62251 Cuernavaca, Morelos, Mexico

Received 26 September 1997, in final form 20 November 1997

Abstract. Absolute differential and total cross sections for single-electron loss and capture were measured from Ar^+ ions on He in the energy range of 1.0–5.0 keV. The reduced differential cross sections ($\rho = (d\sigma/d\Omega)\theta \sin\theta$ versus $E_{lab}\theta = \tau$) are shown to scale reasonably well for each of the two processes studied. For single-electron loss, our cross sections are found to be of the order of magnitude of 10^{-19} cm^2. An extrapolation of the high-energy results to low energies shows good agreement with the present data. The total cross section for single-electron capture is compared with other available measurements. These results give a general shape of the whole curve of single-electron capture cross sections for the Ar^+–He system over a wide range of energy.

1. Introduction

Currently, single-electron loss and capture processes for some species in collision with helium at keV energies are of considerable interest (Atan *et al* 1991, Wu *et al* 1988, 1989). Important motivations result particularly from the need to understand the mechanism of energy and particle loss in magnetically confined plasmas and their application to the pumping of argon ion lasers (Tsuji *et al* 1993). A survey of the data (Wu *et al* 1988, 1989) indicates that there are few published measurements for the Ar^+–He system over a wide energy range but to our knowledge, no previous theoretical and experimental studies of this system have been made in the low-keV energy range. Sen and Li (1993) have measured the single-electron capture cross sections for this system in the energy range 50–250 keV and they display a decreasing behaviour of the data with increasing energy. Nikolaev *et al* (1961) reported a measurement of the cross section at 1.4 MeV. Mahadevan and Magnuson (1968) have measured the cross section below 200 eV.

Also to our knowledge there is only one reported measurement of the single-electron loss cross sections in collisions between Ar^+ and He. Only Sen and Li (1993) have measured this cross section at high energies (50–250 keV). Recently, Kamber *et al* (1993) used translational energy spectroscopy to detect Ar^{2+} ions by means of state-selective single-electron loss processes of ground state and highly excited metastable Ar^+ ions in collisions with He.

This lack of information was one of the reasons for the investigations reported in this paper, where we present absolute measurements of the differential and total cross sections of single-electron loss and capture for Ar^+ collisions with He atoms. The energy range covered by the present study is 1.0–5.0 keV.

0953-4075/98/071553+10$19.50

2. Experiment

An apparatus to measure angular distributions (Martínez and Hernández 1997, Martínez *et al* 1997) consists basically of three parts: an ion source, a scattering chamber and a detection system. Figure 1 shows a general scheme of the apparatus used. The Ar^+ ions were formed in an arc discharge source containing Ar gas (99.99% purity) at ion source pressures of 0.05–0.08 mTorr. Ions were extracted and accelerated to 1.0–5.0 keV. The intensity of the Ar^+ beam extracted at 5.0 keV is typically of 5.0×10^{-7} A. Because beam collimation is used in this apparatus, the current available for the experiment is only $\approx 5.0 \times 10^{-9}$ A. The Ar^+ beam is passed through an einzel-type lens and directed to a Wien velocity filter in order to obtain an analysed beam at the desired velocity. Next, the Ar^+ ions are passed between cylindrical electrostatic deflection plates which were used both to steer the beam and to bend it by 10° to prevent photons in the ion source from reaching the detection system. The Ar^+ beam crosses the neutralization chamber (which is not used in this experiment) whose slits served as collimators. Then, the collimated Ar^+ beam entered the scattering chamber, which housed a gas target cell where the loss and capture phenomena to form Ar^{2+} and Ar^0 took place. The gas target cell was a cylinder of length 2.54 cm and diameter 2.54 cm in which the target gas pressure (typically 0.4 mTorr) was measured with a calibrated MKS capacitance manometer (model 270C). The entrance aperture was 1 mm in diameter and the exit aperture was 2 mm wide and 6 mm long. This geometry permitted the measurements of the Ar^{2+} and Ar^0, the directions of which make an angle of up to $\pm 7^\circ$ with respect to the incoming beam direction. Path lengths and apertures were chosen such that the root-mean-square angular resolution of the system was $\approx 0.1^\circ$. All apertures and slits had knife edges. The target cell was located at the centre of a rotatable, computer-controlled vacuum chamber that moved the whole detector assembly, which was located 47 cm away from the target cell. A precision stepping motor ensured a high repeatability in the positioning of the chamber over a large series of measurements. The detector assembly consisted of a Harrower-type parallel-plate analyser (Harrower 1955) with a 0.36 mm entrance aperture

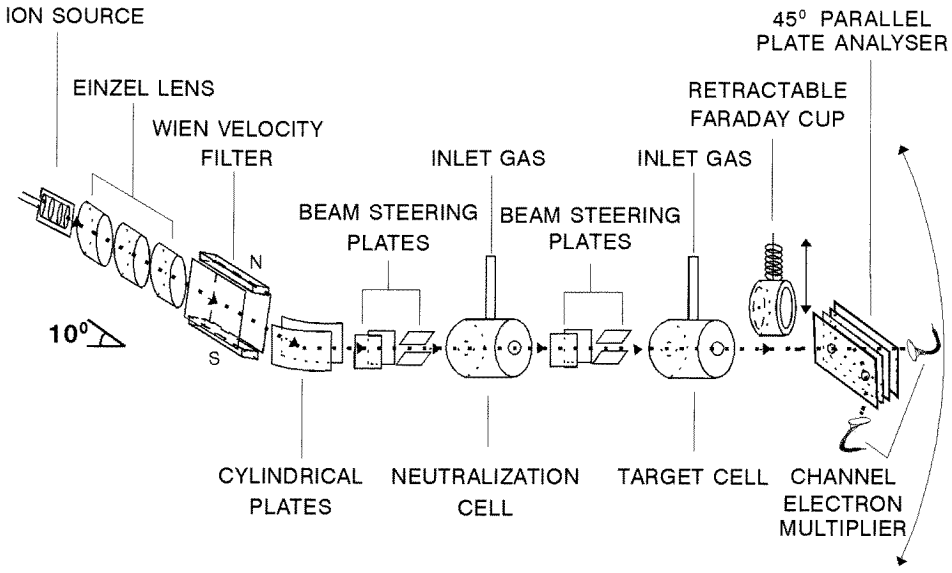

Figure 1. Schematic diagram of the apparatus.

and two channel-electron multipliers (CEMs) attached to its exit ends. The beam entered the uniform field of the analyser at an angle of 45°. The neutral beam (Ar^0) passed straight through the analyser through a 1 cm orifice on its rear plate and impinged on a CEM so that the neutral counting rate could be measured (typically $\sim 1.4 \times 10^4$ particles/s). Separation of charged particles occurred inside the analyser, which was set to detect the Ar^{2+} ions with the lateral CEM (typically ~ 900 particles/s). The multiplier counting efficiencies for Ar^{2+} and for Ar^0 were assumed to be the same as H^+ at the same energy. All the experimental data have been corrected for counting efficiency (Crandall *et al* 1975). A retractable Faraday cup was located 33 cm away from the target cell, allowing the measurement of the incoming Ar^+ ion-beam current (typically $\sim 5.0 \times 10^{-10}$ A). A Keithley Instruments Electrometer model 610C was used to measure the beam current entering the Faraday cup. Vacuum base pressures in the system were 2.0×10^{-7} Torr without gas in the cell and 1.0×10^{-6} Torr with gas.

During the laboratory angular distribution experiment, the collimator in front of the lateral CEM was an orifice of 1 cm in diameter. Under the thin target conditions used in this experiment, the differential cross sections for the formation of Ar^{2+} and Ar^0 were evaluated from the measured quantities by the expression

$$\frac{\mathrm{d}\sigma(\theta)}{\mathrm{d}\Omega} = \frac{I_f(\theta)}{I_0 n l} \tag{1}$$

where I_0 is the number of Ar^+ ions incident per second (typically $\sim 5.0 \times 10^{10}$ particles/s for the Ar^{2+} experiment and $\sim 2.0 \times 10^8$ particles/s for the Ar^0 experiment) on the target; n is the number of helium atoms per unit volume (typically 1.2×10^{13} atoms/cm^3); l, the length of the scattering chamber ($l = 2.5$ cm) and $I_f(\theta)$, the number of Ar^{2+} (or Ar^0) particles per unit solid angle per second detected at a laboratory angle θ with respect to the incident beam direction (typically 1.2×10^9 particles/sr s for Ar^{2+} and $\sim 2.0 \times 10^{10}$ particles/s for Ar^0). The total cross section σ for the production of the Ar^{2+} and Ar^0 particles was obtained by the integration of $\mathrm{d}\sigma/\mathrm{d}\Omega$ over all angles; that is

$$\sigma = 2\pi \int_0^\pi \frac{\mathrm{d}\sigma}{\mathrm{d}\Omega} \sin(\theta)\, \mathrm{d}\theta. \tag{2}$$

Extreme care was taken when the absolute differential cross section was measured. The reported value of the angular distribution was obtained by measuring it with and without gas in the target cell with the same steady beam. Then point-to-point subtraction of both angular distributions was carried out to eliminate the counting rate due to neutralization of the Ar^+ beam on the slits and those arising from background distributions. The Ar^+ beam intensity was measured before and after each scan. Measurements not agreeing to within 5% were discarded. Angular distributions were measured on both sides of the forward direction to ensure they were symmetric. The estimated RMS error was 15%, while the total cross sections were reproducible to within 10% from day to day.

Several runs were made at different gas target pressures and $\mathrm{d}\sigma/\mathrm{d}\Omega$ was determined for each run. These were compared in order to estimate the reproducibility of the experimental results as well as to determine the limits of the 'single-collision regime' since the differential and total cross sections reported are absolute.

In the present work changes were not observed in the absolute values with respect to the ion source conditions. Also, no variation in the distributions were detected over a target pressure range of 0.1–0.7 mTorr.

2.1. Errors

Several sources of errors are present. Possible sources of systematic errors are the following: (i) the effective length of the gas cell (7%); (ii) density determination (9%); (iii) the measurements of the target gas pressure (4%); (iv) the measurement of the incident ion current (5%); (v) the angular resolution (0.1°) and (vi) the detector calibration (3%).

With the assumption of molecular flow, Toburen *et al* (1968) derived a simple way to estimate the effective path length, which is longer than the physical length because of gas streaming from the apertures. This effective increase in path length was estimated to be approximately 3% and then the effective path length was assumed to be equal to the geometrical length of the cell 2.54 cm. The error of the path length from this assumption was estimated to be no more than 7%. The largest source of error in the present measurements arose from the determination of the He density. The target density n is determined from the target gas pressure and temperature. The total uncertainty was estimated to be of the order of 7%. The Ar^+ beam intensity was measured before and after each scan. Measurements not agreeing to within 5% were discarded, and a total uncertainty of 5% was estimated. The CEMs could be calibrated *in situ* with a low-intensity Ar^{2+} beam, which could be measured as a current in a Faraday cup by a sensitive electrometer. The uncertainty in the detector calibration was estimated to be less than 3%. Although data were corrected to account for most of these uncertainties, the absolute error of the reported cross sections is believed to be less than $\pm 15\%$. This estimate represents both random and systematic errors.

The relative accuracy or reproducibility is found to be better than 10%.

3. Results and discussion

Measurements of differential cross sections (DCSs) have been performed at laboratory angles of $-4^\circ \leqslant \theta \leqslant 4^\circ$ and collision energies of $1.0 \leqslant E_{\mathrm{lab}} \leqslant 5.0$ keV.

3.1. For single-electron loss

Figure 2 exhibits angular and energy dependence (the reduced differential cross section, $\rho = (\mathrm{d}\sigma/\mathrm{d}\Omega)\theta \sin\theta$) of the single-electron loss differential cross sections in the laboratory system, where the abscissa is the reduced angle $\tau = E_{\mathrm{lab}}\theta$. In order to make figure 2 clear, horizontal error bars were put only on some data. Four features of the reduced cross section curves are worthy of remark: first, $\rho(\tau)$ has a rather similar behaviour at all energies to within the experimental uncertainty and it depends strongly on the angle and energy at small reduced angles for $\tau < 1.0$ keV deg; second, the curves at high energies (3, 4 and 5 keV) show a tendency to fall into a single pattern, while the curves of low-energy data clearly fall over different curves; third, it increases rapidly with τ up to a maximum which is located near 1.0 keV deg for 1 keV, at 1.9 keV deg for 2 keV and 4.0 keV deg at high energies. This maximum becomes sharper as the energy decreases and is followed, in some cases, by very slight oscillations which confirm the existence of a curve crossing; finally, for the 1.0 keV data a systematic shift is observed between the low- and the high-energy curves. The measured differential cross sections for single-electron loss of Ar^+ impact on He have been integrated over the observed angular range, and are shown in figure 3 and listed in table 1. The error bars are a measure of the reproducibility of the data (10%). Figure 3 shows a comparison between the present data and the results at high energies (Sen and Li 1993). Our cross sections are found to be of the order of magnitude of 10^{-19} cm^2. An extrapolation of the high-energy results to low energies shows good agreement with the present data. The

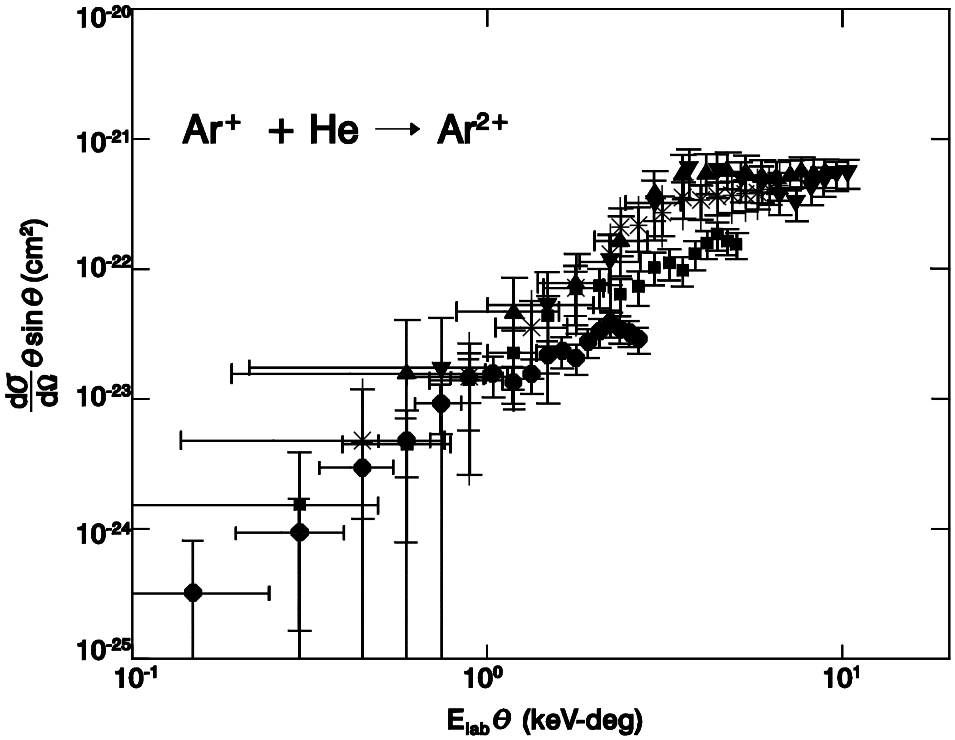

Figure 2. Reduced differential cross sections for single-electron loss of Ar^+ ions in He. ●, 1.0 keV; ■, 2.0 keV; ∗, 3.0 keV; ▲, 4.0 keV; ▼, 5.0 keV.

full curve in figure 3 represents a least-squares fit of a fourth-order polynomial function using the high-energy results (Sen and Li 1993) and the present data. The shape of the total cross section shows a monotonically increasing behaviour as a function of the incident energy. This behaviour can be explained qualitatively in terms of momentum transfer and projectile–target interaction time. For energies smaller than E_{max} (the energy at which the cross section is maximum) a smaller momentum can be transferred to the projectile electrons as the energy of the projectile decreases (Atan *et al* 1991). From the least-squares fit it is found that $\sigma_{12} \sim E^2$ in the energy range $1 \leqslant E \leqslant 20$ keV. A similar behaviour had been found by Kaneko (1985), who using the unitarized impact parameter method to calculate the electron loss cross section for He^+ ions colliding with He, N_2, Ar and Kr, found that $\sigma_{12} \sim E^{2.8}$ in the energy range $30 \leqslant E \leqslant 150$ keV; no remarkable differences in the energy dependence of σ_{12} could be found for any atom. We know that these are different collision systems but can be used to make a comparison of the behaviour of the cross sections as a function of the impact energy. The difference in the energy dependence of the present data and Kaneko's (1985) calculations can be explained based on the fact that the projectiles are different. It also has to be considered that in ion–atom collisions the interaction probabilities are strongly influenced by the electronic structures of the exciting partner and projectile; the Kaneko (1985) calculation gives a better agreement with the data, in the region where the impact velocity $v \sim Z_1 v_0$ (Z_1 is the atomic number of the projectile and v_0 is the Bohr velocity) as well as for hydrogen-like ions.

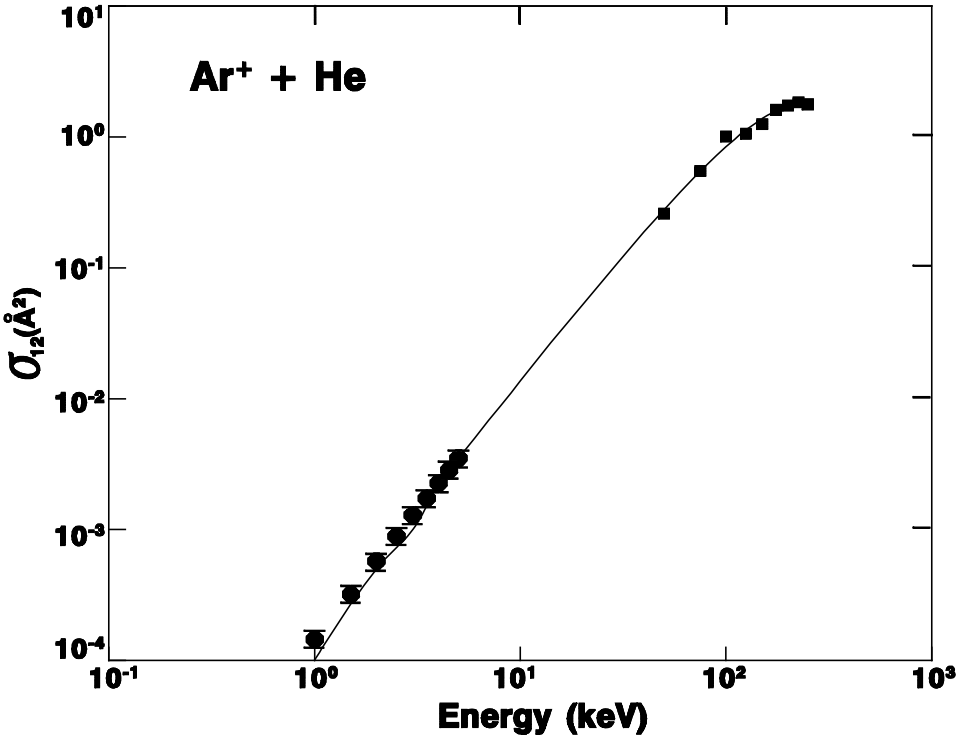

Figure 3. Total cross sections for single-electron loss of Ar^+ ions in He. ●, present measurements; ■, Sen and Li (1993). The full curve represents a least-squares fit of a fourth-order polynomial function using both Sen and Li's (1993) data and present results.

3.2. For single-electron capture

Characteristic reduced differential cross sections for single-electron capture of Ar^+ ions in He for different values of the incident energy are presented in figure 4. In order to make figure 4 clear, horizontal error bars were only put on some data. Several remarkable features can be observed which are worth pointing out: (i) as in the single-electron loss case, $\rho(\tau)$ has a similar behaviour at all energies within experimental uncertainty and it depends strongly on the angle and energy at small reduced angles for $\tau < 2.0$ keV deg; (ii) the curves at high energies (3, 4 and 5 keV) show a tendency to fall into a single pattern, while the curves for low-energy data clearly follow different curves; (iii) it increases rapidly with τ up to a maximum which is located near 3.5 keV deg for 1.0 keV, at 4.5 keV deg for 2.0 keV and 7.5 keV deg at high energies. This maximum becomes sharper as the energy decreases; (iv) from the 1.0 keV data a systematic shift is observed between the low-energy curves and the high-energy curves; (v) the tail of the curves at high energy shows a tendency to fall out in a single pattern.

Plotted in figure 5 and listed in table 1 are the total cross sections for single-electron capture obtained by integration of the angular distributions as a function of the impact energy. The error bars are a measure of the reproducibility of the data (10%). We have included data over a wide range of energies (Sen and Li 1993, Mahadevan and Magnuson 1968, Nikolaev *et al* 1961) to show the overall shape of the curve. It can

Table 1. Cross sections for single-electron loss and capture of Ar^+ on He.

Energy (keV)	σ_{12} (Å^2)	σ_{10} (Å^2)
0.0849		$0.006\,74 \pm 0.001\,35$[a]
0.0851		$0.011\,9 \pm 0.002\,4$[a]
0.0892		$0.025\,6 \pm 0.005\,1$[a]
0.0937		0.157 ± 0.031[a]
0.0986		$0.094\,7 \pm 0.018\,9$[a]
0.119		0.161 ± 0.032[a]
0.149		0.225 ± 0.045[a]
0.179		0.211 ± 0.042[a]
1.0	$0.000\,14 \pm 0.000\,01$	0.72 ± 0.07
1.5	$0.000\,32 \pm 0.000\,03$	0.96 ± 0.10
2.0	$0.000\,57 \pm 0.000\,06$	1.28 ± 0.13
2.5	$0.000\,89 \pm 0.000\,09$	1.44 ± 0.14
3.0	$0.001\,28 \pm 0.000\,13$	1.52 ± 0.15
3.5	$0.001\,73 \pm 0.000\,17$	1.76 ± 0.18
4.0	$0.002\,26 \pm 0.000\,23$	1.87 ± 0.19
4.5	$0.002\,84 \pm 0.000\,28$	1.92 ± 0.19
5.0	$0.003\,51 \pm 0.000\,35$	2.00 ± 0.20
50.0	0.26 ± 0.02[b]	2.21 ± 0.37[b]
75.0	0.55 ± 0.04[b]	1.62 ± 0.27[b]
100.0	1.01 ± 0.12[b]	1.84 ± 0.33[b]
125.0	1.06 ± 0.05[b]	1.52 ± 0.24[b]
150.0	1.25 ± 0.1[b]	1.34 ± 0.21[b]
175.0	1.61 ± 0.12[b]	1.38 ± 0.24[b]
200.0	1.74 ± 0.13[b]	1.61 ± 0.27[b]
225.0	1.84 ± 0.11[b]	1.34 ± 0.24[b]
250.0	1.78 ± 0.14[b]	1.14 ± 0.19[b]
1400.0		0.561 ± 0.168[c]

[a] Mahadevan and Magnuson (1968).
[b] Sen and Li (1993).
[c] Nikolaev *et al* (1961).

be seen from figure 5 that our data may connect the results at low energies of Mahadevan and Magnuson (1968) with those of Sen and Li (1993) at high energies. Although there is no overlap of the four sets of data, the shapes of the cross section data of Sen and Li (1993), Mahadevan and Magnuson (1968), Nikolaev *et al* (1961) and present measurements, indicate that the data from all four measurements are mutually consistent. These results give a general shape of the whole curve of single-electron capture cross sections for the Ar^+–He system over a wide range of energies (0.0849–1400 keV). In an attempt to compare our measurements with theoretical calculations, we made a review and found no calculations for this process. However, in order to obtain a preliminary understanding of the trend of the total cross sections, we considered the behaviour of some of these cross sections in the intermediate energy range as illustrated in the following using the semiempirical model of Olson (1970). The total single-electron cross sections are then calculated with the universal reduced cross section of Olson (1970) using the parameters of Smith *et al* (1970) ($R_c = 2.9\ a_0$, $|\Delta V'(R_c)| = 5.2$ eV a_0^{-1} and $\Delta E = 4.7$ eV) and $H_{12} = 1.33$ eV, which were fitted until the experimental cross section at 3.0 keV was obtained. The results of this calculation are shown in figure 5 (full curve). Although the Olson model calculations are not expected to be highly reliable, the calculation of σ_{10} is seen to agree in shape with

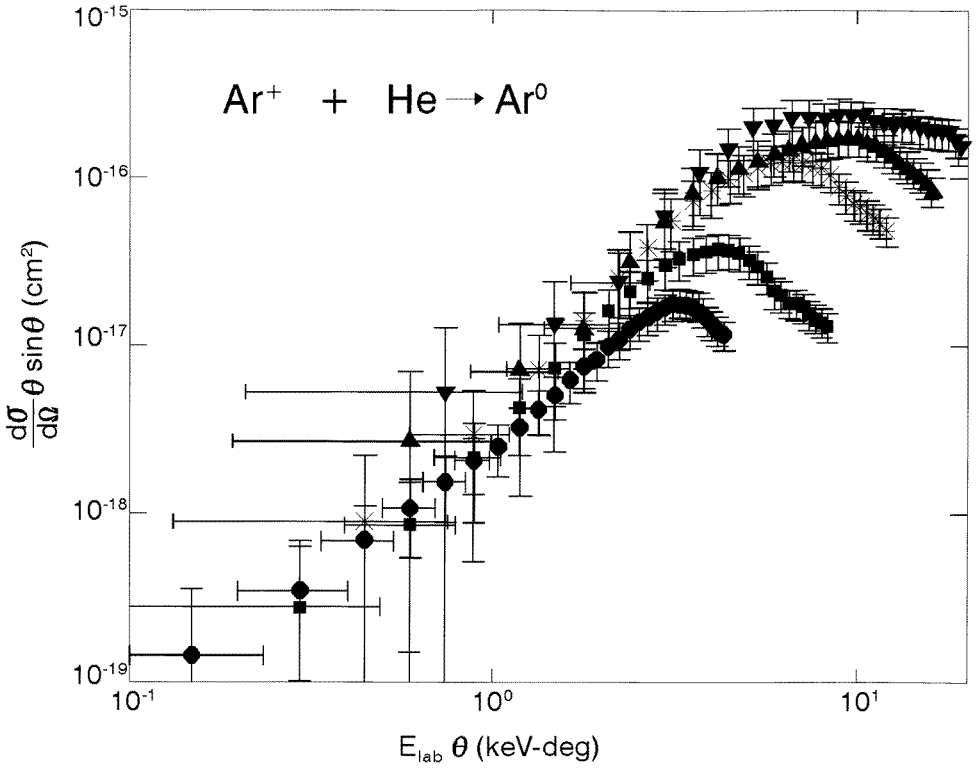

Figure 4. Reduced differential cross sections for single-electron capture of Ar^+ ions in He. ●, 1.0 keV; ■, 2.0 keV; ∗, 3.0 keV; ▲, 4.0 keV; ▼, 5.0 keV.

the present measurements over the entire energy range within experimental uncertainties. At low energies, the experimental data of Mahadevan and Magnuson (1968) lie above the Olson model calculation, with deviations of ∼100%, while those of Sen and Li (1993) at high energies have deviations of ∼60%.

It may be noted that the energy dependence of the cross sections for single-electron loss and capture may be influenced by the presence of the excited states of the Ar^0, Ar^+ and Ar^{2+} ions. In these cases, it has been suggested (Sen and Li 1993, Kamber *et al* 1993) that the production of Ar^0 and Ar^{2+} may be influenced by the presence of the excited states of the projectile Ar^+ and the final particles Ar^{2+} and Ar^0, which were produced by single-electron loss and capture, respectively.

Up to now, there has been no theoretical study dealing with the above two processes to compare with our experimental results in this energy range. It thus appears desirable that a detailed theoretical analysis should be carried out to further investigate this behaviour.

In summary, we have reported experimental observations of the absolute differential and total cross sections for single-electron loss and capture of Ar^+ in He at impact energies between 1.0 and 5.0 keV.

For single-electron loss, our cross sections are found to be of the order of magnitude of 10^{-19} cm^2. An extrapolation of the high-energy results to low energies shows good agreement with the present data.

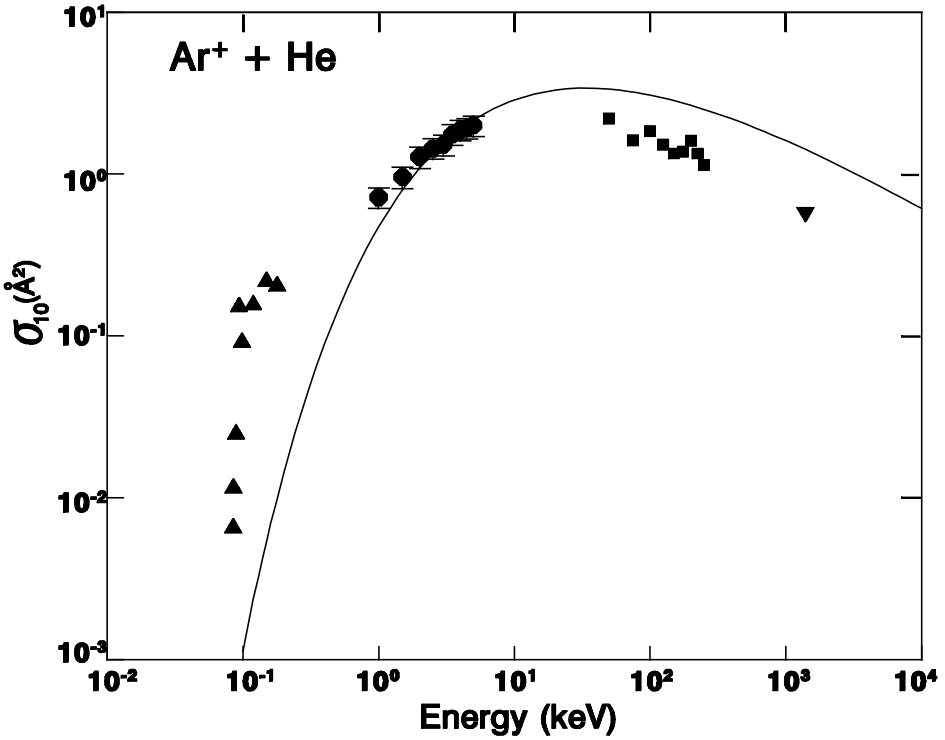

Figure 5. Total cross sections for single-electron capture of Ar^+ ions in He. ●, Present measurements; ■, Sen and Li (1993); ▼, Nikolaev *et al* (1961); ▲, Mahadevan and Magnuson (1968); ——, Olson (1970).

The total cross section for single-electron capture is compared with other available measurements. These results give a general shape of the whole curve of single-electron capture cross sections for the Ar^+–He system over a wide range of energy.

Acknowledgments

We are grateful to B E Fuentes and I Domínguez for helpful suggestions and comments, and to P G Reyes for his technical assistance. Research supported by DGAPA IN-100392 and CONACyT 3659P-E9607.

References

Atan H, Steckelmacher W and Lucas M W 1991 *J. Phys. B: At. Mol. Opt. Phys.* **24** 2559–69
Crandall D A, Ray J A and Cisneros C 1975 *Rev. Sci. Instrum.* **46** 562–4
Harrower G A 1955 *Rev. Sci. Instrum.* **26** 850–4
Kamber E Y, Enos C S and Brenton A G 1993 *Nucl. Instrum. Methods* B **79** 71–4
Kaneko T 1985 *Phys. Rev.* A **32** 2175–85
Mahadevan P and Magnuson G D 1968 *Phys. Rev.* **171** 103–9
Martínez H and Hernández J M 1997 *Chem. Phys.* **215** 285–9
Martínez H, Hernández J M, Reyes P G, Marquina E R and Cisneros C 1997 *Nucl. Instrum. Methods* B **124** 464–8
Nikolaev V S, Dmitriev I S, Fateeva L N and Teplova Ya A 1961 *Sov. Phys.–JETP* **13** 695–702
Olson R E 1970 *Phys. Rev.* A **2** 121–6

Sen A and Li Xi 1993 *Nucl. Instrum. Methods* B **79** 44–9
Smith F T, Fleischmann H H and Young R A 1970 *Phys. Rev.* A **2** 379–96
Toburen L H, Nakai M Y and Langley R A 1968 *Phys. Rev.* **171** 114–22
Tsuji M, Kaneko N, Furusawa M, Muraoka T and Nishimura Y 1993 *J. Chem. Phys.* **98** 8565–71
Wu W K, Huber B A and Wiesemann K 1988 *At. Data Nucl. Data Tables* **40** 57–200
——1989 *At. Data Nucl. Data Tables* **42** 157–85